J Nanopart Res (2011) 13:6149–6155
DOI 10.1007/s11051-011-0294-2

SPECIAL ISSUE: NANOSTRUCTURED MATERIALS 2010

Reconstitution of aluminium and iron core in horse spleen apoferritin

G. Ciasca · M. Chiarpotto · G. Campi · B. Bocca · M. Rodio · A. Pino · A. Ricci · N. Poccia · C. Rossi · A. Alimonti · H. Amenitsch · P. De Sole · A. Bianconi

Received: 13 September 2010 / Accepted: 11 February 2011 / Published online: 18 March 2011

Abstract This study investigates the uptake of iron and aluminium by apoferritin. In particular, we provide the first evidence that apoferritin is able to bind in vitro the physiological form of aluminium, $Al(OH)_4^-$, to reach an Al/Fe atomic ratio of about 0.15. Mass spectrometry analysis shows that the Al content increases linearly as a function of Al concentration in solution. These findings provide a better understanding of the Al uptake in vivo, confirming that the metal content of ferritin depends on the metal bio-availability.

Keywords Aluminium · Metal toxicity · Ferritin · SAXS · ICP-MS · Nanomedicine

G. Ciasca and M. Chiarpotto have contributed equally to this work.

G. Ciasca (✉) · M. Rodio · A. Ricci · N. Poccia · A. Bianconi
Dipartimento di Fisica, Università degli Studi "La Sapienza", P.zzale Aldo Moro, 5, 00185 Rome, Italy
e-mail: gabriele.ciasca@uniroma1.it

M. Chiarpotto · C. Rossi · P. De Sole
Dipartimento di Biochimica e Biochimica Clinica, Università Cattolica del Sacro Cuore, Largo Agostino Gemelli, 8, 00168 Rome, Italy

G. Campi
CNR, Institute of Crystallography, Via Salaria Km 29.300, 00016 Monterotondo, RM, Italy

B. Bocca · A. Pino · A. Alimonti
Dipartimento di Ambiente e Connessa Prevenzione Primaria, Istituto Superiore di Sanità, Via Regina Elena, 00161 Rome, Italy

H. Amenitsch
Institute of Biophysics and X-ray Structure, Research, Austrian Academy of Sciences, Steyrergasse 17/VI, 8010 Graz, Austria

Introduction

Ferritin is the main iron storage protein in living systems. Mammalian ferritins are composed of 24 subunits of two different type: "H" i.e., heavy chain and "L" i.e., light chain. Subunits are assembled in a octahedral (432) symmetry, forming a soluble hollow sphere with an internal and external radii of about 3.5 and 7 nm, respectively (Harrison 1996). Subunits pack tightly together except at three fold axes and four fold axes, where narrow channels traverse the protein shell. Three fold channels are mainly hydrophilic, being lined with six negatively charged residues, whereas four fold channels are mainly hydrophobic (Douglas and Ripoll 1998). Ferritin cavity is able to store up to 4500 iron (Fe) atoms as an inorganic complex (i.e. the ferrihydrite). The mechanism of iron uptake and storage into the ferritin cavity has been extensively studied in the literature (Harrison 1996). The main steps are the following: (i) Fe(II) migration across the three fold hydrophilic

channels; (ii) Fe(II) oxidation catalyzed by H subunits; and (iii) iron oxide core formation assisted by L subunits.

Although ferritin has its main role in iron storage, several experimental evidences demonstrate that it is able to bind also in vivo other metals, such as aluminium (Al) (Joshi et al. 1989 Grady 2000, Fleming and Joshi 1991). In this context, in a recent study on some groups of patients, Spada et al. (2009) have observed that serum ferritin contains thousands of Al atoms besides iron and zinc atoms. As shown by inductively coupled plasma mass spectrometry (ICP-MS) measurements, the Al/Fe molar ratio of serum ferritin ranges from $\sim$0.6 to $\sim$6.5 and can be correlated with the clinical conditions of subjects (Spada et al. 2008, 2009). These results could open the way to the development of new diagnostic tools based on the measurements of the aluminium content of serum ferritin. To this purpose, providing a clear understanding of the mechanism of metal binding to ferritin is of great importance.

In this article, we present a study of Al and Fe uptake by apoferritin providing the first compelling evidence that apoferritin is able to bind in vitro the negatively charged $Al(OH)_4^-$, i.e. the physiological form of Al, to reach a maximum atomic Al/Fe ratio of about 0.15. Al uptake has been induced incubating apoferritin in several solutions containing an Al salt in the presence of a Fe salt at different pH values. The incubated apoferritin Al content has been studied by means of ICP-MS. Small angle X-ray scattering (SAXS) has been used to study the structural features of samples incubated in the presence of Fe and Al at different pH values. The measurements show the integrity of the apoferritin shell after the incubation in a reaction solution far from physiological pH and, at the same time, provide an effective method for monitoring the mineralization process of the apoferritin core upon incubation.

Materials and methods

Protein preparation

All the experiments have been carried out using horse spleen apoferritin (ApoFt) purchased from Sigma. ApoFt was incubated overnight at 25 °C in several reaction solutions containing an iron salt ($FeSO_4 \cdot 7H_2O$) and an aluminium salt ($AlK(SO_4)_2 \cdot 12H_2O$), both at the nominal concentration of 0.6 mM.

As Al solubility is strongly decreased by the precipitation of $Al(OH)_3$ at neutral pH (Martin 1986) different actual concentrations of aluminium in solution have been obtained controlling the solution pH in the range 6.5–8.9. Incubation procedure was as follows. Four TRIS 0.1 M buffer solutions at different pH values, namely 6.5, 7.4, 8.5 and 8.9, containing both the iron and the aluminium salts were prepared; in these solutions, actual soluble Fe and Al concentrations are lower than the nominal salt concentration (0.6 mM), as a consequence of Al and Fe precipitation as hydroxide. Final concentrations were measured by mass spectroscopy and the results are reported in Table 1. Thirty microliters of apoferritin solution 0.1 mM was added to 10 ml of supernatant fluids harvested from each saline solutions. Final apoferritin concentration was 0.3 μM. The reaction solutions was incubated overnight. After incubation, apoferritin has been separated from the reaction solution using centrifugal concentrators produced by Sartorius (product number VS0612, mass cutoff 5 kDa, protein recovery >96%). Thus, the protein has been diluted in a TRIS buffer solution at the proper pH. Several centrifugation and dilution cycles have been performed to completely eliminate residual Al and Fe contents in the apoferritin solution (i.e., Al and Fe not bonded to apoferritin). Incubated apoferritin Al and Fe contents have been determined by ICP-MS.

ICP MS measurements

Metal ion contents (Al, Fe) bonded to the apoferritin molecule were measured by sector field ICP-MS,

Table 1 ICP-MS results

Solution pH	[Al] in solution (μM)	[Fe] in solution (μM)	Nunber of Al/ApoFt	Nunber of Fe/ApoFt
6.50 ± 0.05	1.5 ± 0.3	500 ± 80	1.3 ± 0.5	520 ± 50
7.40 ± 0.05	15 ± 8	450 ± 80	1.5 ± 0.5	170 ± 20
8.50 ± 0.05	100 ± 20	200 ± 50	18 ± 6	270 ± 30
8.90 ± 0.05	260 ± 50	70 ± 15	36 ± 8	280 ± 30

Column 1 incubation solutions pH, *Columns 2, 3* Al and Fe concentrations into the incubation solutions, *Columns 4,5* number of Al and Fe atoms mineralized into the apoferritin cavity upon incubation

using the ELEMENT 2 model from Thermo Fisher (Bremen, Germany) in the medium resolution mode ($m/\Delta m = 4000$). The isotopes chosen for quantification were ^{27}Al for aluminium and ^{56}Fe for iron. The medium resolution approach allows to separate the analytical peaks from the interfering ones (i.e., $^{13}C^{14}N$, $^{12}C^{15}N$, $^{54}Fe^{++}$, and $^{11}B^{16}O$ on mass 27; and $^{40}Ar^{16}O$ and $^{40}Ca^{16}O$ on mass 56). The system was equipped with a torch guard electrode device, platinum interface cones, and a standard sample introduction apparatus, i.e., a Meinhard type glass nebulizer with water-cooled Scott chamber. The following operating conditions were used: radio frequency power, 1.2 kW; argon flow rates, 14.0 L/min (plasma), 0.90 L/min (auxiliary), and 0.85 L/min (nebulizer). To quantify the elements a 1:20 (v/v) dilution with high-purity deionized water was used. The standard addition approach was adopted for calibrations and ^{115}In was used as internal standard at a concentration of 1 ng/mL in analytical solutions. Calibrants were daily prepared from single-element stock solutions of 1 mg/L (Spex Industry, Edison, NJ, USA) by dilution with high purity deionized water. The sensitivity of the method calculated as three fold the standard deviation of repeated measurements of blanks was 0.1 ng/mL for Al and 0.2 ng/mL for Fe. Each determination was in quadruplet and the mean value used. The value of blank (apoferritin incubated in absence of Fe and Al salt) was subtracted from all samples. To allow for an accurate background subtraction, i.e., to evaluate the residual amount of Al and Fe atoms, the centrifugation dilution cycle was performed also in the absence of apoferritin.

SAXS measurements and data analysis

SAXS measurements were carried out on the Austro SAXS beamline at the Synchrotron Radiation Facility ELETTRA (Trieste, Italy) (Amenitsch et al. 1997). Samples have been measured in a 2-mm-diameter capillary sample holder. Incident X-ray energy was fixed at 8 keV. Data acquisition has been performed with an image plate detector Mar 345 in a q range 0.01–5 nm^{-1}. To allow for accurate subtraction of the background scattering, solvent scattering was acquired before and after measuring the protein solutions. The 2D SAXS pattern was azimuthally averaged, using the program FIT 2D to obtain the scattered intensity I(q) as a function of the X-ray-exchanged momentum q. Each acquisition was averaged over 500 s to optimize signal-to-noise ratio and avoid sample damage. Measurements were performed at room temperature.

I(q) curves have been processed by the indirect transform program GNOM (Svergun 1992) to evaluate the pair distribution function (PDF) on the overall interval [0, D_{max}], where $D_{max} = 16$ nm has been fixed for each samples.

A 3D low-resolution bead-model of the incubated apoferritin has been produced using the simulated annealing method implemented in the program DAMMIN (Svergun 2001). Fifteen independent 3D DAMMIN reconstructions were averaged by the program DAMAVER to obtain the model of each incubated apoferritin (Volkov and Svergun 2003).

Following the method proposed by Galvetz and co-workers (Galvetz et al. 2008), we computed the bead-counting histogram for each incubated apoferritin, calculating the radial distance R between the center of mass of the particle and each bead of the structural file produced by DAMAVER. Histogram bin size was fixed at 0.7 nm. Each bin frequency, f(R), was normalized by the quantity $V(R) = 4/3\pi(R^3_{max}–R^3_{min})$, where R_{max} and R_{min} are, respectively, the upper bound and the lower bound of the bin centered on the radial distance R. This normalization takes properly into account that the bead counting at distance R is directly proportional to the volume, V(R), of an hollow sphere centered on R and whose thickness is equal to the bin size.

Results and discussion

Al and Fe uptake by apoferritin

In Table 1 the number of Al and Fe atoms bonded to apoferritin, measured by ICP-MS, are shown together with the measured concentrations of both metals in the reaction solutions at different pH. As clearly shown, the number of Fe atoms per ferritin molecule is greater than the number of Al atoms by one or two orders of magnitude.

In Fig. 1a the number of Al atoms per ferritin molecule (Al/ApoFt) is plotted versus the solution pH: a rather exponential curve is obtained. This trend can be easily explained taking into account the chemistry of Al in water solution: while below pH 5 aluminum

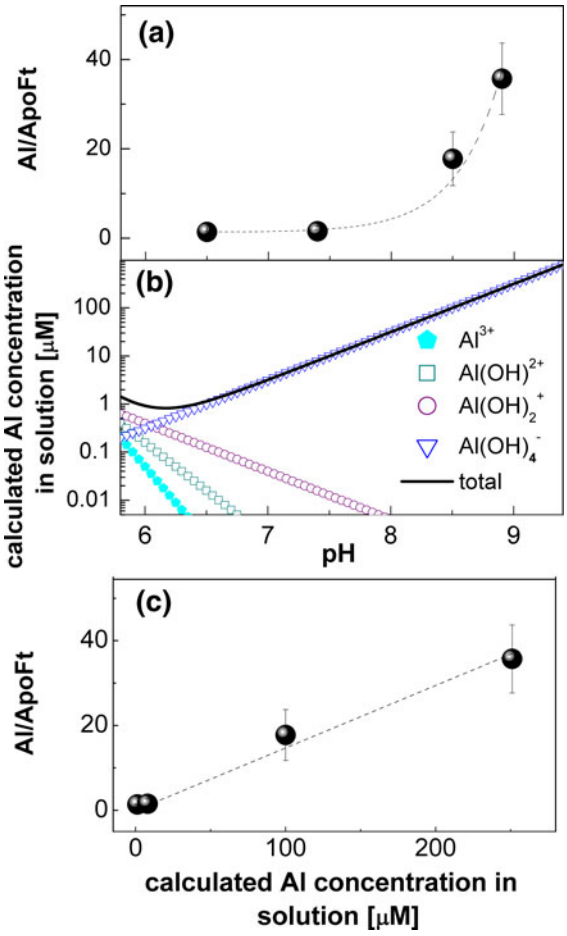

Fig. 1 **a** Number of Al atoms mineralized into the apoferritin cavity (Al/ApoFt) as a function of the solution pH, **b** concentration of Al ionic species in water solution as a function of pH values (a semi-log scale is used). Concentrations have been calculated according to the method reported in (Martin 1986), **c** number of mineralized Al atoms (Al/ApoFt) plotted against Al concentration in the reaction solution calculated in Fig. 2c

exists as Al^{3+}, at pH 5–6 different Al species are present such as Al^{3+}, $Al(OH)^{2+}$ and $Al(OH)_2{}^{+}$. These ions precipitate as $Al(OH)_3$ and redissolve above pH 6 forming $Al(OH)_4{}^{-}$ (Martin 1986).

In Fig. 1b, the theoretical concentrations of soluble Al species permitted by the $Al(OH)_3$ solubility at different pH are shown[1] (Martin 1986). Comparing the calculated behavior of Al in solution (Fig. 1b) with the trend observed in Fig. 1a, it is clear that apoferritin is able to bind the physiological form of Al in solution, i.e., the negatively charged $Al(OH)_4{}^{-}$. As, indeed, shown in Fig. 1b, above pH 6.5, the only soluble Al species is $Al(OH)_4{}^{-}$, and its concentration grows exponentially with pH. On the contrary, the concentrations of Al^{3+}, $Al(OH)^{2+}$, and $Al(OH)_2{}^{+}$ are negligible (in general, significantly lower than 0,1 μM that corresponds to a maximum of one Al atom per ten apoferritins) and decreases exponentially with pH. All these data are consistent with the uptake of the negatively charged $Al(OH)_4{}^{-}$.

In Fig. 1c, we report the number of Al atoms per ferritin molecule (previously shown in Fig. 1a) versus the Al concentration into to the reaction solution calculated in Fig. 1b. The number of Al atoms increases linearly with the Al concentration in solution. This result suggests a simple explanation of the trend displayed in Fig. 1a, i.e., the dependency of the number of bonded Al atoms on pH arises from the relation between pH and Al concentration in the incubation solution. In other words, Fig. 1c strongly suggests that the main limiting factor for Al uptake during the iron core reconstruction is the Al concentration in solution.

Morphological characterization of the incubated apoferritin

In this section, the structural features of the incubated apoferritin samples are studied by Small Angle X-ray Scattering, which provides an effective methods for monitoring the metal uptake process.

In Fig. 2 (left panels), we report the scattering patterns of the native (panel a) and incubated apoferritins (panels c,e,g). Panels are sorted in the ascending order of the metal content (Table 1), irrespectively of pH. Dramatic changes in the

[1] Concentrations displayed in Fig. 1b, have been calculated algebraically solving the following system of chemical reactions: $\mathbf{Al^{3+} + H_20 \leftrightarrow Al(OH)^{2+} + H^+}, k_d = 10^{-5..5}$,
$\mathbf{Al(OH)^{2+} + H_20 \leftrightarrow Al(OH)_2^+ + H^+}, k_d = 10^{-5.6}$
$\mathbf{Al(OH)_2^+ + H_20 \leftrightarrow Al(OH)_4^- + H^+}, k_d = 10^{-12.1}$
$\mathbf{Al(OH)_3 + 3H^+ \leftrightarrow Al^{3+} + H_20}, k_s = 10^{10.7}$

k_d and k_s indicate the equilibrium dissociation constants and the solubility constant of the Al compounds, respectively, at room temperature.

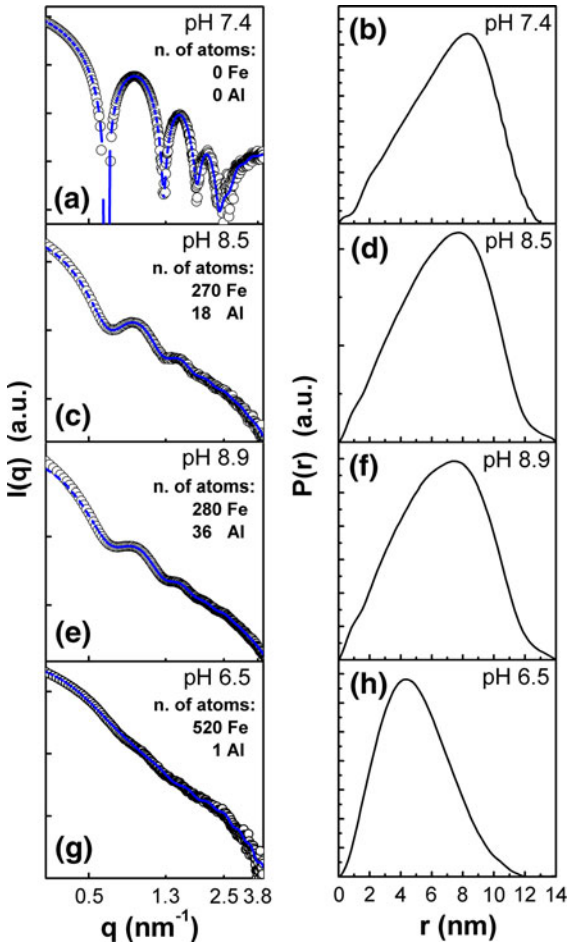

Fig. 2 *Left panels* Scattering profiles of native (panel **a**) and incubated apoferritins (panels **c**, **e**, **g**) as a function of the metal content (a log–log scale is used). The experimental data are displayed as *open dots*. The fits, obtained using the software GNOM, are displayed as *broken lines*; (*right panels*: **b**, **d**, **f**, **h**) Pair distribution functions obtained transforming the SAXS profile by means of the regularized transform software GNOM

I(q) curves can be observed, increasing the metal content within the ferritin cavity.

In Fig. 2 (right panels), we report the corresponding PDF curves obtained after regularized transform of the scattering patterns. In particular, Fig. 2b shows the PDF of an apoferritin solution at physiological pH. Figure 2d, f, and h show the PDF curves of the incubated samples at pH 8.5, 8.9 and 6.5, respectively. As the metal content increases, a shift of the PDF maximum toward lower values due to an increase of the PDF contribution around 4 nm can be observed. As demonstrated by Galvetz and coworkers (Galvetz et al. 2008), the ferritin PDF signal around 4 nm is dominated by the excess electronic density of the metal core, whereas the signal around 8 nm is dominated by the excess electronic density of the protein shell. Comparing the curve in Fig. 2b with the remaining PDF curves, it appears that incubation induces a re-mineralization of the apoferritin cavity.

To gain a better knowledge about the structure of the incubated samples, we analyze the scattering patterns with the simulated annealing method DAMMIN. Results are summarized in Fig. 3. Panels a, b, c, and d show the 3D DAMMIN models corresponding to the PDF curves reported in Fig. 2, i.e. an empty apoferritin (Fig. 3a) and the incubated samples at pH 8.5, 8.9, and 6.5 (Fig. 3 b, c, d). Panels e, f, g, h report a cross section of each 3D DAMMIN model passing trough the protein center. Panels i, j, k, and l show the normalized bead counting histogram as a function of the distance from the core centre (R). This quantity has been calculated as described in "Materials and Methods".

The 3D DAMMIN models (Fig. 3 a, b, c, d) show that our incubation procedure does not result in dramatic changes of the low-resolution shape of the protein shell (i.e., size and spherical symmetry of the molecule are conserved), confirming that the incubation in a reaction solution far from physiological pH does not induce protein unfolding or aggregation. An inspection of the cross-sectional shape as a function of the ferritin metal content (Fig. 3 e, f, g, h) suggests that the mineralization process starts from the outer shell and proceeds toward the center of the cavity. In particular, in Fig. 3e, we show the cross section of an empty apoferritin sample. For $R < 3.6$ nm, a hole in the cross section can be clearly observed, corresponding to the empty cavity of apoferritin. An increase in the metal content results first in a reduction of the hole radius (Fig. 3f) and then its complete disappearance (Fig. 3h). The normalized bead-counting histogram of the incubated samples as a function of metal content confirms the mechanism described above. For low-metal content (Fig. 3j), bead counts vanish for $R < 0.8$, whereas they are not null for $R > 0.8$ nm. As the metal content increases (Fig. 3k, l), the cavity center begins to be filled and, at the same time, the outer part of the core becomes more dense.

It is worth noting that the proposed core–shell analysis can be performed only if the apoferritin metal content is low (i.e. several hundreds of iron

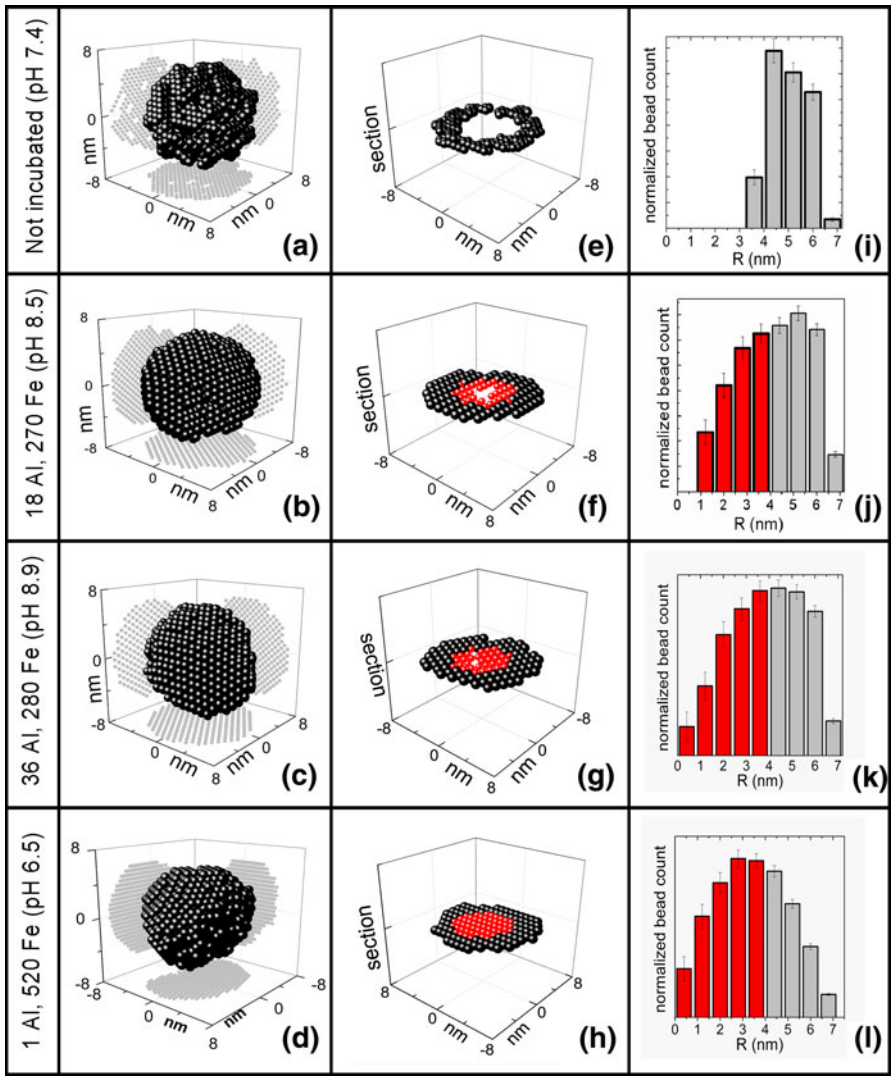

Fig. 3 It is organized as a table; each row is referred to a different apoferritin sample. Rows are sorted in the ascending order of the apoferritin metal content (Table 1), irrespective of pH. In the header column of the table (on the left), the apoferritin metal content of each sample is reported together with the solution pH values. **a**, **b**, **c**, **d** show the 3D model of the apoferritin samples obtained with DAMMIN: **e**, **f**, **g**, **h** show the corresponding cross sections of the 3D models and **i**, **j**, **k**, **l** show the bead counting histogram obtained by the 3D models. Different colours have been used for the core and the shell. (Color figure online)

atoms). When the apoferritin cavity is completely filled, the contribution of the shell became completely negligible with respect to the contribution of the inorganic metal core and reconstructing the low-resolution shape of the shell becomes harder. Full model refinement for SAXS data analysis is currently under construction.

Conclusion

In this article, we have studied in vitro the binding of Al to apoferritin, focusing our attention on the behavior of Al in its ionic forms. We have induced Al uptake incubating empty apoferritin in a reaction solution containing Fe and Al salts; as Al solubility is strongly decreased by the precipitation of $Al(OH)_3$ at neutral pH, we obtained different Al concentrations in solution simply controlling the solution pH in the range of 6.5–8.9. In this range (Fig. 1b), aluminium can be found only in its physiological forms, i.e., as the negatively charged $Al(OH)_4^-$.

In our experimental system, Fe uptake by apoferritin is rather independent from the pH of reaction solution, while Al uptake is controlled by pH. This result is highly interesting especially in consideration

of the very high content of aluminium found in serum ferritin of healthy blood donors (Spada et al. 2008). Further experimental studies are in progress to evaluate the relationship between ferritin and aluminium in pathological conditions.

The effectiveness of our procedure has been tested by SAXS measurements, showing that incubation in the reaction solutions actually results in a re-mineralization of the apoferritin cavity and the change in pH does not induce dramatic protein aggregation or unfolding.

As demonstrated by our ICP-MS measurements, the number of Al content per ferritin molecule has a rather exponential behavior with pH, providing the first explicit evidence that apoferritin is able to bind the physiological form of Al in solution, i.e., the negatively charged $Al(OH)_4^-$. This is a notable finding because apoferritin is known to bind preferentially positively charged ions (Yang and Chasteen 1996; Takahashi 2003). Furthermore, the number of mineralized Al atoms into the ferritin cavity increases linearly as a function of Al concentration in the protein environment. This result strongly supports one of the hypotheses suggested in our previous papers (Spada et al. 2008, 2009), i.e., that the concentration of metal atoms found into the serum ferritin cavity is related to the bioavailability of the metals.

In conclusion, we hope that this study gives new insights for understanding better the mechanism behind aluminum uptake in vivo into the ferritin cavity.

References

Amenitsch H, Bernstorff S, Kriechbaum M, Lombardo D, Mio H, Rappolt M, Laggner P (1997) Performance and first results of the ELETTRA high-flux beamline for small-angle x-ray scattering. J Appl Crystallogr 30:872–876. doi:10.1107/S0021889897001593

Douglas T, Ripoll DR (1998) Calculated electrostatic gradients in recombinant human h-chain ferritin. Protein Science 7:1083–1091. doi:10.1002/pro.5560070502

Fleming J, Joshi J (1991) Ferritin: The role of aluminium in ferritin function. Neurobiology of Aging 12(5):413–418. doi:10.1016/0197-4580(91)90066-S

Galvetz N, Fernandez B, Sanchez P, Cuesta R, Ceolin M, Clemente-Leon M, Trasobares S, Lopez-Haro M, Calvino JJ, Stephan O, Dominguez-Vera JM (2008) Comparative structural and chemical studies of ferritin cores with gradual removal of their iron contents. J Am Chem Soc 130(25):8062–8068. doi:10.1021/ja800492z

Grady J (2000) Vanadyl (iv) binding to mammalian ferritins. an epr study aided by site-directed mutagenesis. Journal of Inorganic Biochemistry 80:107–113. doi:10.1016/S0162-0134(00)00046-5

Harrison P (1996) The ferritins: molecular properties, iron storage function and cellular regulation. Biochim Biophys Acta 1275:161–203. doi:10.1016/0005-2728(96)00022-9

Joshi J, Sczekan S, Fleming J (1989) Ferritin a general metal detoxicant. Biol Trace Elem Res 21:105–110. doi:10.1007/BF02917242

Martin FB (1986) The chemistry of aluminium as related to biology and medicine. Clin Chem 32: 1797–1806. (URL http://www.clinchem.org/cgi/content/abstract/32/10/1797)

Spada PL, Rossi C, Alimonti A, Bocca B, Cozza V, Ricerca B, Bocci M, Vulpio C, De Sole P (2008) Ferritin iron content in haemodialysis patients: Comparison with septic and hemochromatosis patients. Clin Biochem 41:997–1001. doi:10.1016/j.clinbiochem.2008.05.003

Spada PL, Rossi C, Alimonti A, Bocca B, Ricerca BM, Bocci MG, Carvelli M, Vulpio C, Lucani G, De Sole P (2009) Iron, zinc and aluminium ferritin content of hemodialysis hyperferritinemic patients: comparison with other hyperferritinemic clinical conditions and normoferritinemic blood donors. Clin Biochem 42:1654–1657. doi:10.1016/j.clinbiochem.2009.07.021

Svergun DI (1992) Determination of the regularization parameter in indirect-transform methods using perceptual criteria. J Appl Crystallogr 25:495–503. doi:10.1107/S0021889892001663

Svergun DI (2001) Determination of domain structure of proteins from x-ray solution scattering. Biophys J 80: 2946–2953. doi:10.1016/S0006-3495(01)76260-1

Takahashi T (2003) Functional properties of threefold and fourfold channels in ferritin deduced from electrostatic calculations. Biophys J 84:2256–2263. doi:10.1016/S0006-3495(03)75031-0

Volkov VV, Svergun DI (2003) Uniqueness of ab initio shape determination in small-angle scattering. J Appl Crystallogr 36:860–864. doi:10.1107/S0021889803000268

Yang X, Chasteen N (1996) Molecular diffusion into horse spleen ferritin: a nitroxide radical spin probe study. Biophys J 71:1587–1595. doi:10.1016/S0006-3495(96)79361-X